

PAPER

Study of point defects in wide- bandgap $\text{Cu}_2\text{CdGeS}_4$ microcrystals by temperature and laser power dependent photoluminescence spectroscopy

To cite this article: Jüri Krustok *et al* 2020 *J. Phys. D: Appl. Phys.* **53** 275102

View the [article online](#) for updates and enhancements.



IOP | ebooks™

Bringing together innovative digital publishing with leading authors from the global scientific community.

Start exploring the collection—download the first chapter of every title for free.

Study of point defects in wide- bandgap $\text{Cu}_2\text{CdGeS}_4$ microcrystals by temperature and laser power dependent photoluminescence spectroscopy

Jüri Krustok^{1,2} , Taavi Raadik², Xiaofeng Li², Marit Kauk-Kuusik², Kristi Timmo², Souhaib Oueslati²  and Maarja Grossberg²

¹ Division of Physics, Tallinn University of Technology, Ehitajate Tee 5, Tallinn 19086, Estonia

² Department of Materials and Environmental Technology, Tallinn University of Technology, Ehitajate Tee 5, Tallinn 19086, Estonia

E-mail: Juri.Krustok@ttu.ee

Received 27 January 2020, revised 12 March 2020

Accepted for publication 26 March 2020

Published 5 May 2020



Abstract

We present temperature and laser power dependent photoluminescence (PL) study of high quality wide-bandgap $\text{Cu}_2\text{CdGeS}_4$ microcrystals. At $T = 10$ K three PL bands were detected at about 1.919 eV (#1), 1.855 eV (#2) and 1.748 eV (#3). The temperature and laser power dependencies indicate that the properties of PL bands can be explained by donor- acceptor pair model, where the #1 and #2 bands result from a recombination between distant pairs involving the same shallow acceptor V_{Cu} with $E_A \approx 30$ meV and different deep donor defects. The #3 PL band originates from the deep donor-deep acceptor pair recombination where the depth of deep acceptor defect is more than 157 meV. Detailed analysis of the PL spectra show the absence of deep potential or band gap fluctuations in this material making it suitable for photovoltaic applications.

Keywords: photoluminescence, donor-acceptor pairs, defects, $\text{Cu}_2\text{CdGeS}_4$, wide bandgap

(Some figures may appear in colour only in the online journal)

1. Introduction

Earth-abundant, inexpensive and non-toxic materials for thin film solar cell technologies are attracting considerable attention due to the growing need for environmentally friendly and sustainable sources of renewable energy. Thin film solar cells have the key benefit of their dimensionality, having thickness of a fraction of crystalline silicon solar cells making them appealing in terms of cost factor with minimum material usage. The most advanced thin film solar cell technologies today are $\text{Cu}(\text{In,Ga})\text{Se}_2$, CdTe , and organic-inorganic hybrid perovskites. All of them have achieved over 20% conversion efficiency on the laboratory scale. Although reaching high solar cell device efficiencies, these materials face various problems limiting their wider commercial availability, high cost being one of these issues. Therefore, the search

for cheaper materials based on abundant elements has directed the scientific community to kesterite compounds such as $\text{Cu}_2\text{ZnSnS}_4$, $\text{Cu}_2\text{ZnSnSe}_4$ and $\text{Cu}_2\text{ZnSn}(\text{S,Se})_4$. These semiconductors have a direct band gap, high absorption coefficient values exceeding 10^4 cm^{-1} , p-type conductivity and a tailored band gap in the range of 1.0–1.5 eV [1]. Unfortunately, the record conversion efficiency of kesterite solar cells is still below 13% [2].

As a possible solution to increase the efficiency of thin film solar cells, the tandem structures are recommended, where the top cell has a larger band gap and thus expands the spectral sensitivity range of a single junction solar cell toward higher photon energies. This tandem structure concept is well known for thin film solar cells based on group III–V compound semiconductors and is mostly used for space applications. However, the tandem cell concept can also be used for other solar

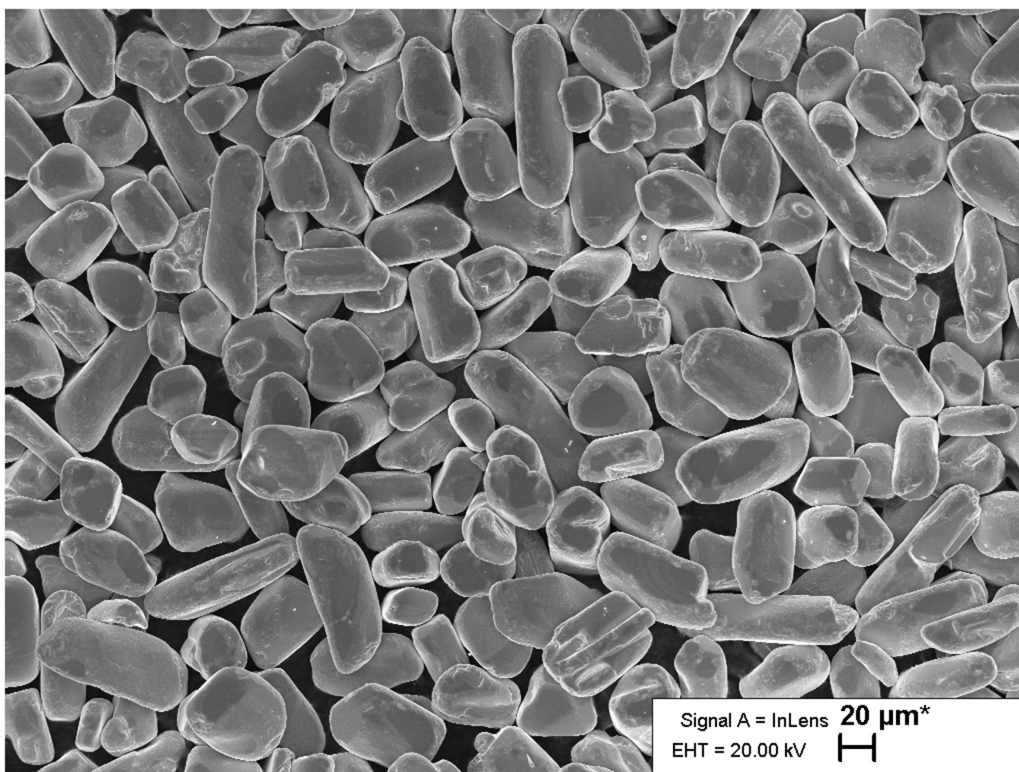


Figure 1. SEM image of CCGS microcrystals.

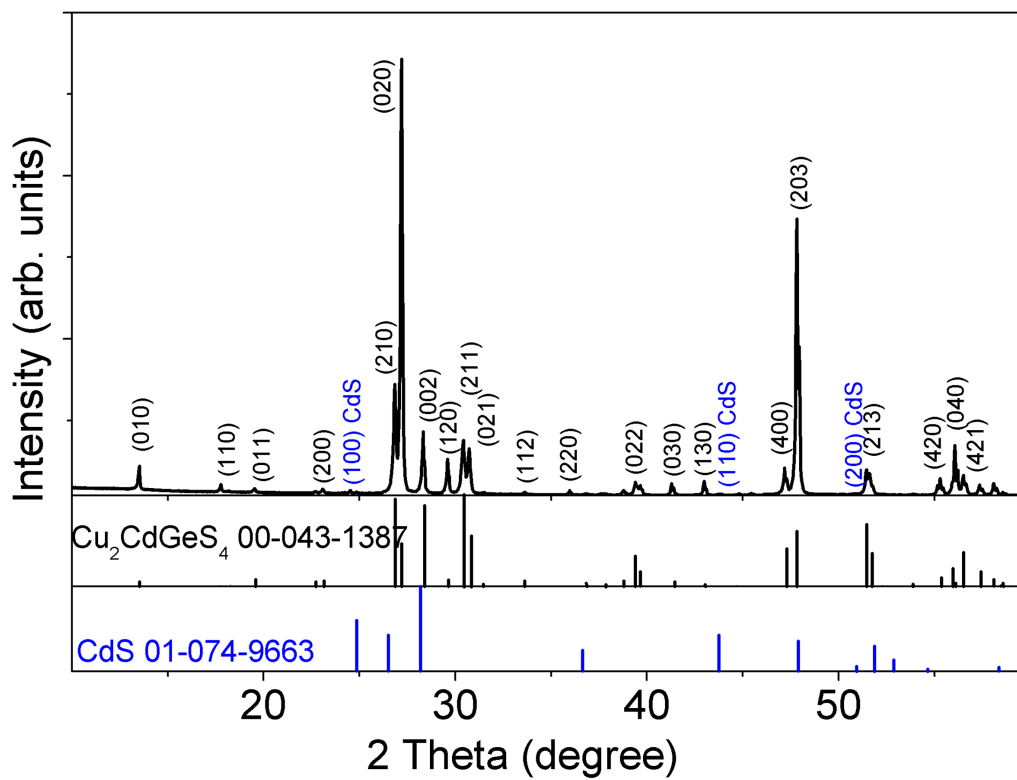


Figure 2. X-ray diffraction pattern of $\text{Cu}_2\text{CdGeS}_4$ microcrystals. Reference ICDD card data for CCGS and CdS are also shown.

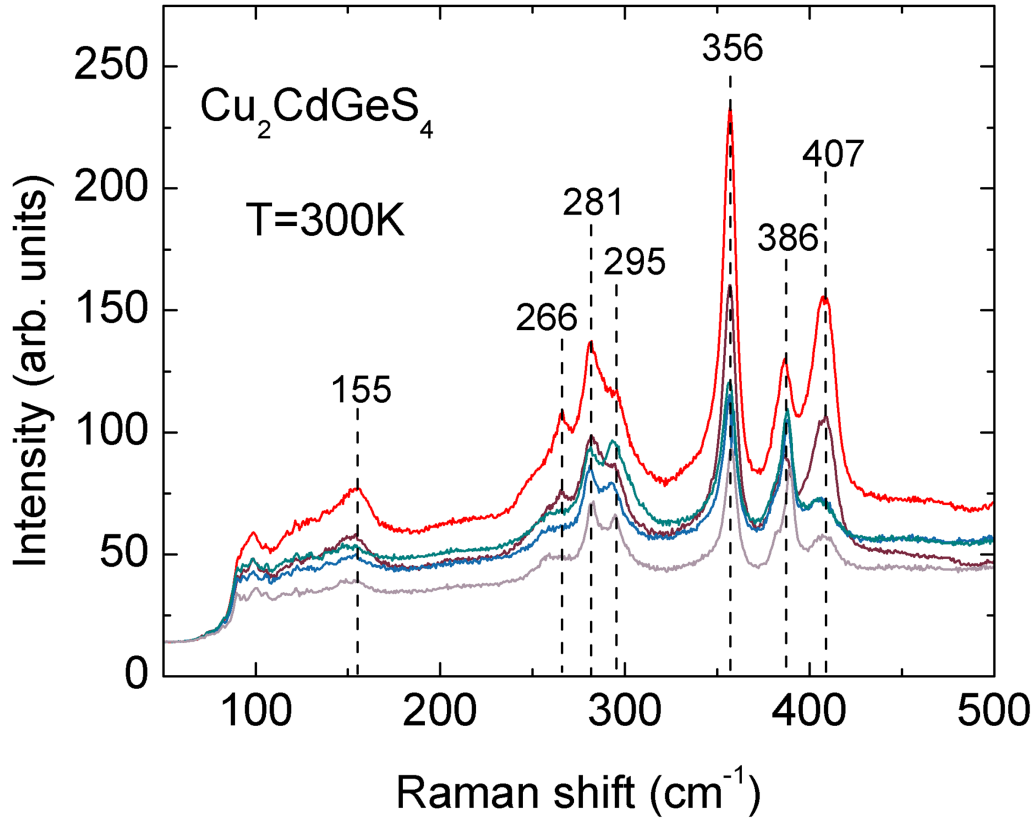


Figure 3. Room temperature Raman spectra of different CCGS microcrystals.

cells. Latest studies have shown that the $\text{Cu}_2\text{ZnGe}(\text{S},\text{Se})_4$ compound could be a good candidate for top cell in Si-wafer-based devices [3]. Theoretical calculations have also shown that by using $\text{Cu}_2\text{ZnSnS}_4/\text{Cu}_2\text{ZnSnSe}_4$ tandem structures even the efficiency of kesterite solar cells can be increased up to 22% [4]. However, the band gap energy of $\text{Cu}_2\text{ZnSnS}_4$ is only 1.5 eV and in many cases that is too low for the top cell. Therefore, a direct larger band gap compound for the top cell is needed having a natural p-type conductivity, high absorption coefficient and is preferably with low concentration of intrinsic defects. It is known that in $\text{Cu}_2\text{ZnSnS}_4$ the defect concentration is usually relatively high causing potential (and band gap) fluctuations and reducing the carrier mobility and lifetime [5–7]. Our recent studies have shown that the average depth of potential fluctuations due to charged defects in an orthorhombic quaternary compound $\text{Cu}_2\text{CdGeS}_4$ is smaller than in kesterites- only about 20 meV [8, 9]. It is expected that similar relatively small potential fluctuations are also present in orthorhombic $\text{Cu}_2\text{CdGeS}_4$ (CCGS) compound and due to higher band gap energy, it can be used as a top cell in various tandem structures or as a photoelectrode in photoelectrochemical (PEC) water splitting devices. Unfortunately, there is very little information about defect properties of CCGS. In quaternary compounds even a small deviation from the stoichiometric composition lead to the formation of intrinsic point defects (vacancies, anti-sites, and interstitials), which significantly influences the electrical and

Table 1. Strongest vibrational modes in $\text{Cu}_2\text{CdGeS}_4$ (cm^{-1}).

This work	FTIR data [18]	Raman data [10]
407	407	—
386	389	385–392
356	361	360
295	294	297
281	282	281–284
266	267	266
155	152	148–152

optical properties of the material. As a member of $\text{I}_2\text{-II-IV-VI}_4$ family, the orthorhombic CCGS (space group: $Pmn2_1$) has a crystal structure similar to that of kesterite-structured $\text{Cu}_2\text{ZnSnS}_4$ [10–14]. Reported band gap energy of CCGS varies from 1.85 eV [13] to 2.05 eV [11]. It has already been used as a counter electrode material in dye-sensitized solar cells [15]. In this paper we present first experimental results of defect structure of CCGS studied by temperature and laser power dependent photoluminescence spectroscopy (PL). Low temperature PL is one of the easiest and most sensitive techniques to study the defect structure of semiconductor materials while temperature and laser power dependencies usually give information about the nature of recombination processes.

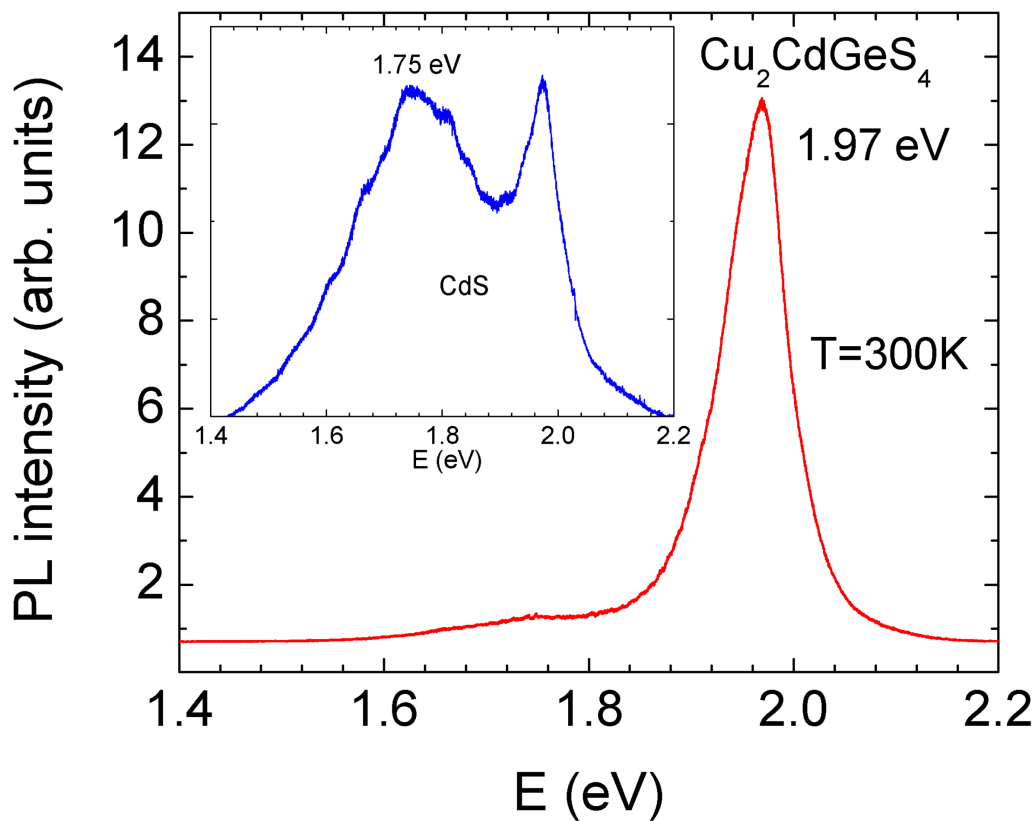


Figure 4. Room temperature micro-PL spectrum measured from single $\text{Cu}_2\text{CdGeS}_4$ microcrystal. The inset shows the micro-PL spectrum from the microcrystal where CdS was dominating.

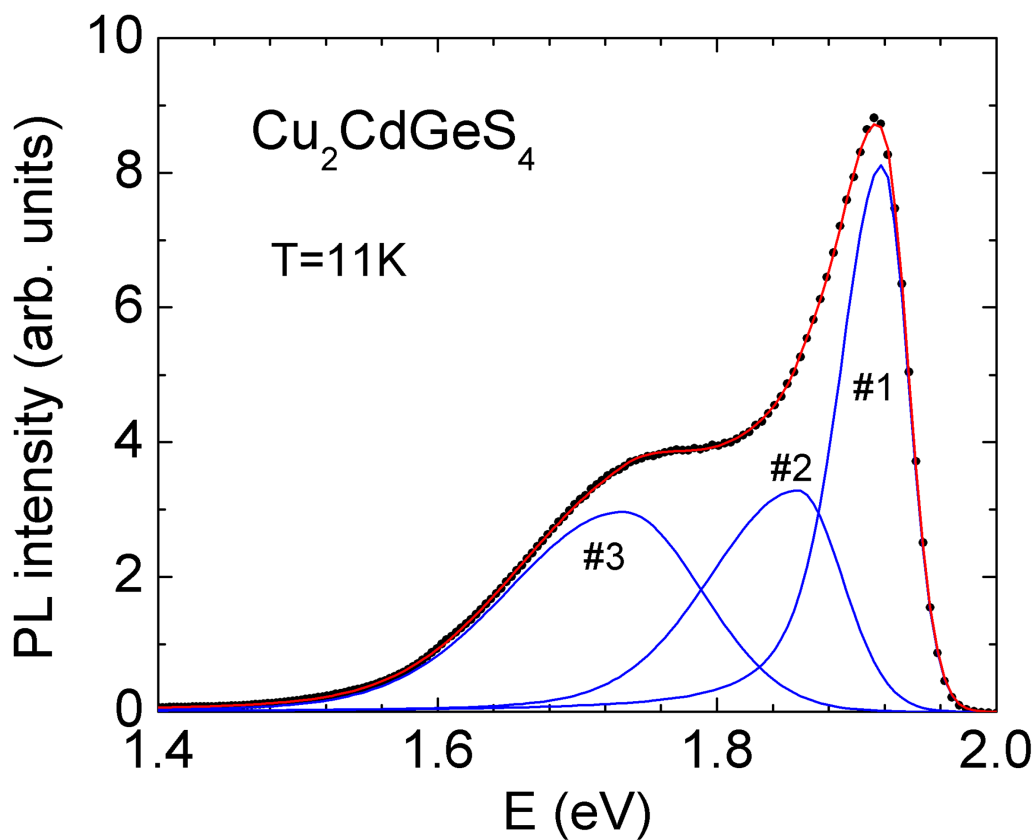


Figure 5. Low temperature PL spectrum of $\text{Cu}_2\text{CdGeS}_4$ microcrystals (dots) and a fitting result (lines) using split Pearson VII function.

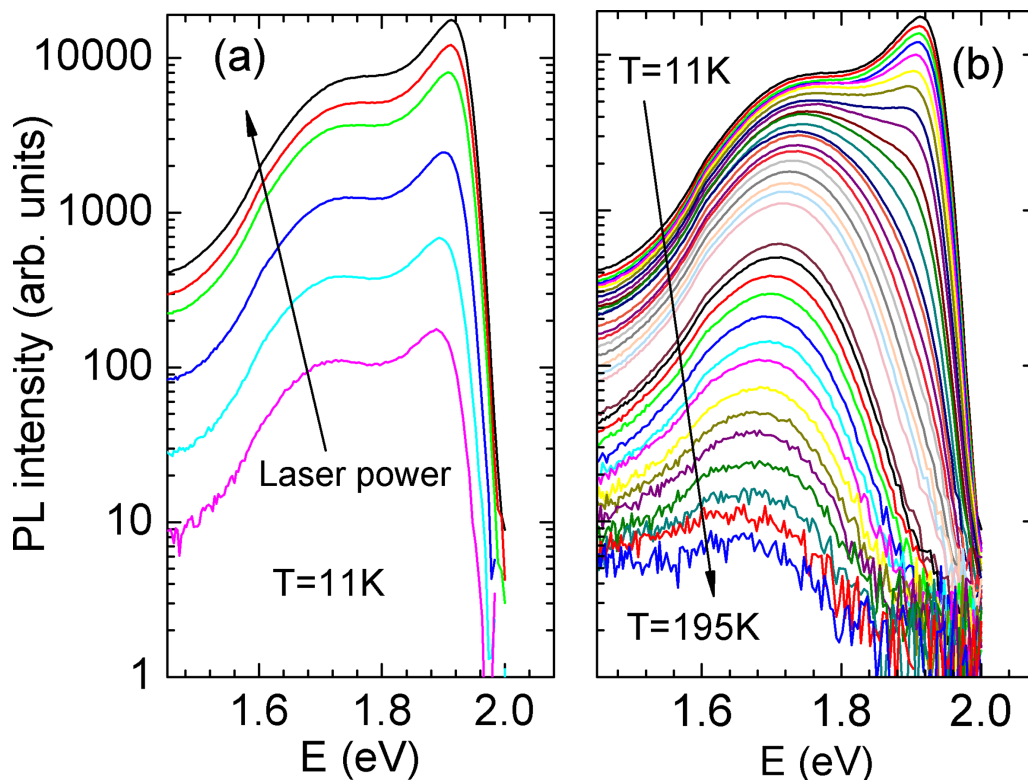


Figure 6. Laser power (a) and temperature dependent (b) PL of $\text{Cu}_2\text{CdGeS}_4$ microcrystals.

2. Experimental

The commercially available CdS powder (5 N purity), elemental Ge powder (5 N purity), S powder (5 N purity) and self-synthesized CuS (5 N purity) were used as reaction precursors to synthesize $\text{Cu}_2\text{CdGeS}_4$ micro-crystalline powder. Potassium iodide (ultra dry, 4 N purity) was used as a molten salt medium. The mass ratio of precursors and salt was 1:1. The starting materials were mixed and loaded into the quartz ampoule in the glovebox to avoid contaminations by air. The ampoule was sealed and then placed into the muffle furnace. The furnace was heated at a rate of 0.5 K min^{-1} to 973 K and then maintained for 120 h. After cooling naturally to room temperature (RT), the as-synthesized powder was removed from ampoule by deionized water. Then, powder was repeatedly washed, dried and sieved to narrow fractions between 38 and $125 \mu\text{m}$, see figure 1. All CCGS microcrystals had a p-type conductivity as determined by the hot probe method. This type of microcrystals are often used in so-called monograin layer solar cells [16].

The crystal structure of the studied CCGS was determined by x-ray diffraction (XRD) using a Rigaku Ultima IV diffractometer with monochromatic Cu K α radiation ($\lambda = 1.5406 \text{ \AA}$) at 40 kV and 40 mA operating with the silicon strip detector D/teX Ultra. The lattice constants were determined using the Rietveld refinement procedure by Rigaku PDXL version 1.4.0.3 software.

The elemental composition of microcrystals was determined by Energy Dispersive x-ray spectroscopy (EDX). The EDX analysis was performed on Zeiss Merlin high-resolution

scanning electron microscope equipped with the Bruker EDX-XFlash6/30 detector. Bulk composition of micro-crystalline powder was measured by EDX from polished crystals. According to EDX results, the average composition of synthesized microcrystals was: Cu (25.1 at. %), Cd (12.8 at. %), Ge (12.0 at. %), S (50.0 at. %).

A 0.64 m focal length single grating (600 mm^{-1}) monochromator and the 442 nm line of a He-Cd laser with different power were used for the PL measurements. For PL signal detection a Hamamatsu R632 PMT was used. A closed-cycle helium cryostat (Janis CCS-150) was employed to measure temperature dependencies of the PL spectra at temperatures from 10 K to 300 K. The crystals under study were glued with cryogenic grease on the cold finger of the cryostat. The laser spot size for these measurements was $200 \mu\text{m}$ in diameter. The sample temperature was controlled using the LakeShore 321 temperature controller.

Raman and micro-PL measurements were carried out using a Horiba LabRAM HR800 Micro-Raman system equipped with a cooled multichannel CCD detection system in the backscattering configuration with a spectral resolution better than 1 cm^{-1} . A YAG: Nd laser (wavelength $\lambda = 532 \text{ nm}$) was used for excitation. The laser spot size was about $2 \mu\text{m}$ in diameter.

3. Results and discussion

Figure 2 shows the resulting x-ray powder diffractogram for the quaternary compound $\text{Cu}_2\text{CdGeS}_4$. $\text{Cu}_2\text{CdGeS}_4$ was

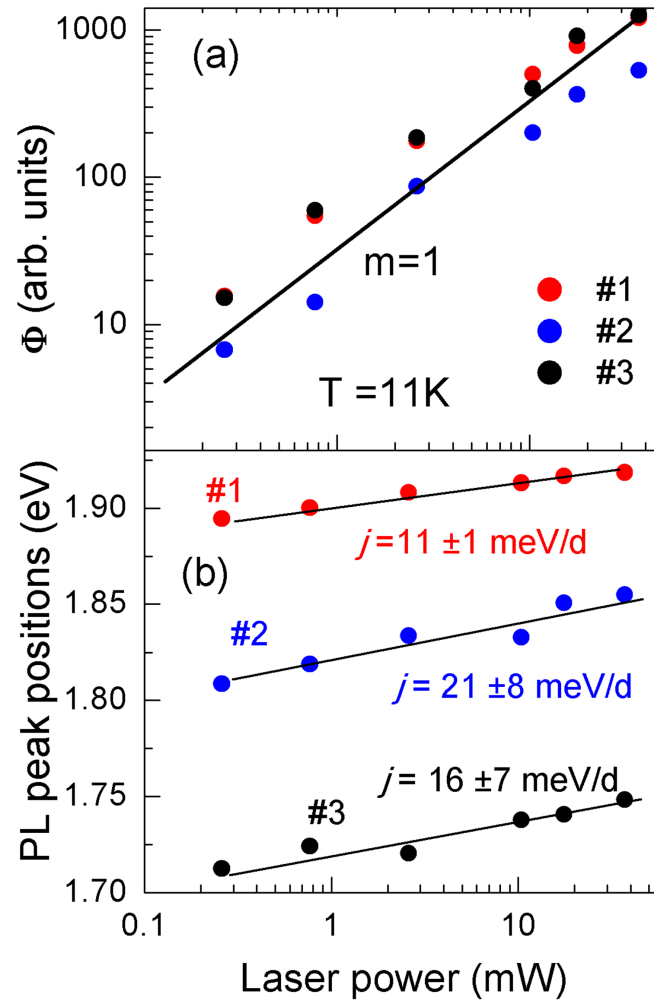


Figure 7. Integrated intensity Φ (a) and peak position (b) of PL bands as a function of laser power at $T = 11$ K. The solid line for $m = 1$ is included for comparison.

found to crystallize in the orthorhombic structure (space group $Pmn21$; ICDD PDF 00-043-1387) with respective lattice parameters $a = 7.7050$ Å, $b = 6.5598$ Å and $c = 6.3025$ Å being in correspondence with data reported by other groups [10, 17]. According to XRD, the $\text{Cu}_2\text{CdGeS}_4$ powder contains less than 1% hexagonal CdS (space group $P63mc$; ICDD PDF 01-074-9663) as a secondary phase.

Raman spectroscopy was used to analyze the phase composition of CCGS microcrystals, see figure 3. While the relative Raman intensity was slightly different, all crystals showed similar peaks. This compound was previously studied by Fourier transform infrared spectroscopy (FTIR) [18] and by low-temperature polarized Raman spectroscopy [10]. Our measured Raman peaks are in good correlation with previously reported vibrational modes in CCGS, see table 1. The full width at half maximum (FWHM) of the most intense 356 cm^{-1} Raman peak is only 4.3 cm^{-1} and this rather small value indicates a good crystal quality of our microcrystals.

We also measured a RT micro-PL from our crystals. The typical PL spectrum is presented in figure 4. The PL band has a slightly asymmetrical shape with a peak position at

$E_{max} = 1.97$ eV. The same emission was also detected in [10], where it was assigned to the band-to-band transition. As a first approximation the peak position of the PL band can be an estimation of the room temperature band gap energy of CCGS: e.g. $\approx E_{max} - (1/2)kT = 1.967$ eV.

In some CCGS crystals, a weak PL band at around 1.75 eV was observed. The 1.75 eV band was more noticeable in separate crystals where CdS was dominating, see the inset in figure 4. According to XRD measurements, a small fraction of CdS is present in our CCGS and although majority of CdS is concentrated on separate crystals (detected also by EDX and Raman), some residues of CdS can also be found on the surface of CCGS microcrystals. Thus, the faint emission at 1.75 eV is proposed to originate from the deep defects in CdS. It is known that Cu doped CdS shows PL emission in the same spectral region [19, 20] and it is probable that we indeed have traces of CdS doped with Cu.

The low temperature PL spectrum of CCGS shows 3 peaks, see figure 5, at 1.919 eV (#1), 1.855 eV (#2) and 1.748 eV (#3). All PL peaks have slightly asymmetrical shape and therefore the best fitting of experimental PL spectra was achieved by

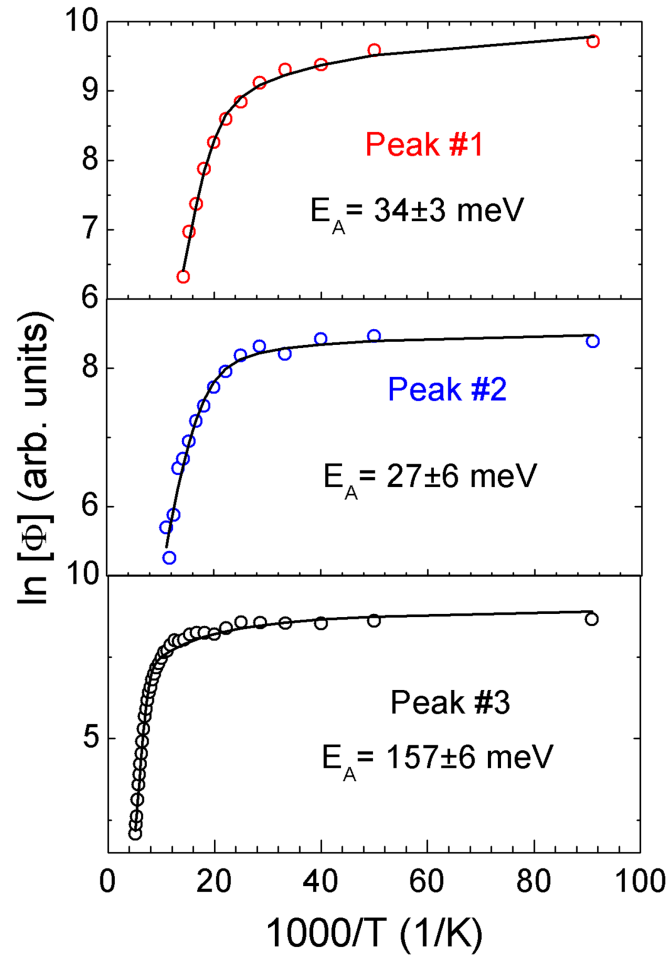


Figure 8. Arrhenius plots for PL bands derived from the temperature dependencies of the PL spectra of CCGS microcrystals. Solid lines present the fitting with the theoretical expression (1).

using split Pearson VII function. The same function was used for all measured PL spectra.

Figure 6 represents the laser power and temperature dependent behavior of PL spectra.

By increasing the laser power, the shape of the PL spectra did not show any dramatic changes, i.e. the integrated intensity Φ of all peaks increase almost linearly with laser power, see figure 7 (a).

The experimental data can be fitted by the simple power law of the form $\Phi \propto L^m$, where Φ is the PL integrated intensity, L is the excitation laser power and m is a dimensionless exponent. It is well known that for an excitation laser photon with an energy exceeding the band gap energy the coefficient m is generally $1 < m < 2$ for the free- and bound-exciton emission, and $m \leq 1$ for free-to-bound and donor-acceptor pair recombinations [21]. Thus, the obtained value of $m \approx 1$ for all bands is a sign that all measured PL bands are related to defects and do not have an excitonic nature. At the same time, all PL bands show a certain blue-shift with laser power, see figure 7 (b). The blue-shift is typical for donor-acceptor (DA) pairs with different distances between donor and acceptor defects in the crystal lattice. The rate of this blue shift is usually higher for DA pairs with shorter distances. Accordingly, the #1 PL

band with a smallest blue-shift of 11 meV per decade of laser power must be related to shallow defects with longest distances between donor and acceptor defects. Sometimes very deep donor and acceptor defects can form DA pairs with a shortest allowed distance between them [22, 23]. These deep donor-deep acceptor (DD-DA) pairs usually do not show any blue-shift with laser power [24, 25]. At the same time, the blue-shift is possible when these DA pairs have slightly different distances between deep donor and deep acceptor defects. Calculated closest interatomic distances in the CCGS lattice are in the ranges 0.2243–0.2320 nm for Ge-S sites, 0.2250–0.2326 nm for Cu-S sites and 0.2520–0.2537 nm for Cd-S sites [14]. These small differences are sufficient to create blue-shift of DD-DA PL bands and can also cause a small asymmetry of PL bands. The blue-shift of PL bands, however, can be caused also by other reasons. In kesterites, for example, wide PL bands at low temperature usually show similar blue-shift with laser power [26] due to high concentration of charged defects, when band tails appear. Typical recombination in kesterites involves holes localized in valence band tail and the blue shift of PL bands is caused by redistribution of holes between tail states [27, 28]. Our CCGS crystals show quite narrow PL band (#1) quite close to the estimated band gap energy. This

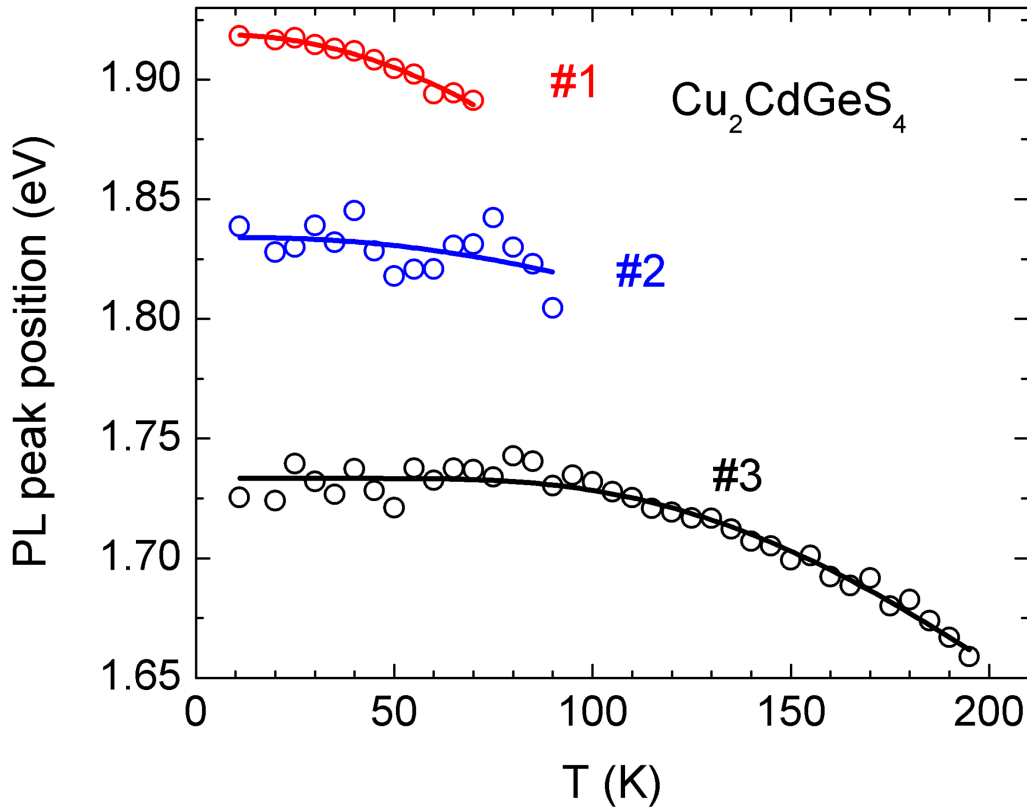


Figure 9. Temperature dependence of the peak positions of the PL bands in CCGS microcrystals.

type of emission is practically impossible in compounds where band tails overlap with shallow defect states. Therefore, the DA pair model seems to be more acceptable to explain the blue-shift of PL bands in the studied CCGS microcrystals.

The thermal activation energies for the bands obtained from the Arrhenius plot (figure 8) where the dependence of $\ln \Phi(T)$ versus $1000/T$ was fitted by using theoretical expression for discrete energy levels [29]:

$$\phi(T) = \phi_0 / \left[1 + A_1 T^{3/2} + A_2 T^{3/2} \exp(-E_A/kT) \right], \quad (1)$$

where Φ is an integrated intensity of the PL band, A_1 and A_2 are the process rate parameters and E_A is the thermal activation energy. As predicted by the fast quenching of the PL bands #1 and #2 with temperature (see figure 6(b)) quite small thermal activation energies $E_A(\#1) = 34 \pm 3$ meV, $E_A(\#2) = 27 \pm 6$ meV were obtained. The deepest PL band (#3) shows the thermal activation energy of $E_A(\#3) = 157 \pm 6$ meV. Small activation energies indicate that relatively shallow defect levels are involved in the recombination processes for PL bands #1 and #2.

All PL bands show a certain redshift with increasing temperature, see figure 9.

The low temperature band gap energy of CCGS is currently not known, but we assume that, like in most quaternary compounds where the band gap energy is increasing with decreasing of temperature, it must be slightly higher than 2 eV.

By combining the thermal activation energies and PL peak positions we are able to generate a low temperature recombination model for CCGS, see figure 10.

According to this model we see, that all PL bands are associated with relatively deep donor levels in the range of 50–120 meV. PL bands #1 and #2 show very comparable thermal activation energies and therefore we propose that they are related to the same shallow acceptor defect. It is known that in kesterites, the most probable shallow acceptor defect is V_{Cu} [30] and it is likely that the same defect is present also in CCGS. The nature of deeper acceptor and donor defects is currently not known and will be a task for future studies. The shallow acceptors detected in this material provide a proof that typical for ordinary kesterites potential or band gap fluctuations play insignificant role in CCGS. Hence, the wide band gap CCGS might very well represent a material that may be used as an absorber in top cells of tandem solar cells or in PEC devices.

4. Conclusion

In conclusion, the results of a detailed photoluminescence study on Cu_2CdGeS_4 microcrystals are presented. Radiative recombination in Cu_2CdGeS_4 microcrystals was studied by temperature and laser power dependent photoluminescence spectroscopy that revealed the origin for the detected low-temperature PL bands at 1.919 eV (#1), 1.855 eV (#2) and 1.748 eV (#3) as donor-acceptor pair recombination. #1 and #2

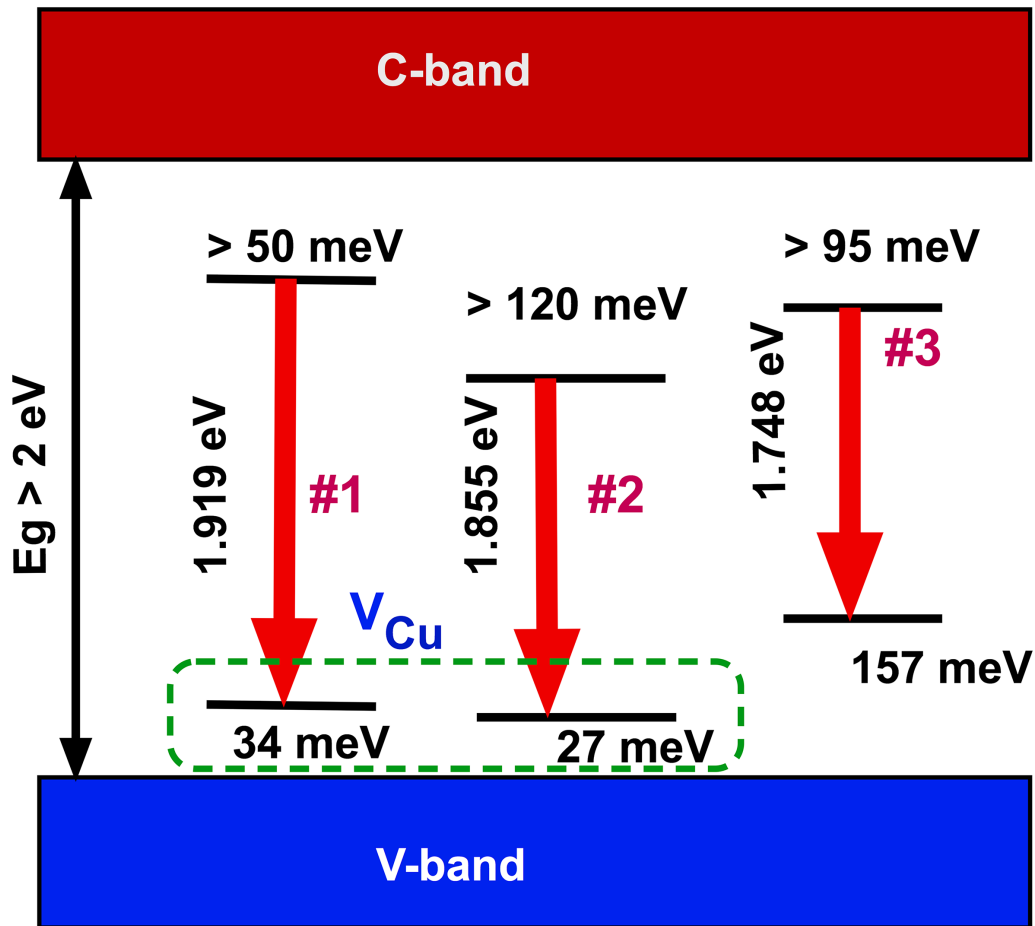


Figure 10. The low temperature recombination model for CCGS microcrystals.

PL bands include more distant donor-acceptor pairs with relatively shallow acceptor (probably V_{Cu}) and deep donor defects. The #3 PL band results from the deep donor—deep acceptor recombination. The manifestation of shallow acceptor defects shows that this material does not have deep potential or band gap fluctuations and could be used in photovoltaic applications.

Acknowledgments

This work has been supported by institutional research funding IUT19-28 of the Estonian Ministry of Education and Research, by the Estonian Research Council grant PSG441, and by the European Regional Development Fund, Project TK141.

ORCID iDs

Jüri Krustok <https://orcid.org/0000-0002-4671-2332>
Souhaib Oueslati <https://orcid.org/0000-0001-7086-9762>

References

- [1] Giraldo S, Jehl Z, Placidi M, Izquierdo-Roca V, Pérez-Rodríguez A and Saucedo E 2019 Progress and perspectives of thin film kesterite photovoltaic technology: a critical review *Adv. Mater.* **31** 1806692
- [2] Wang W, Winkler M T, Gunawan O, Gokmen T, Todorov T K, Zhu Y and Mitzi D B 2014 Device characteristics of CZTSSe thin-film solar cells with 12.6% efficiency *Adv. Energy Mater.* **4** 1301465
- [3] Vermang B *et al* 2019 Wide band gap kesterite absorbers for thin film solar cells: potential and challenges for their deployment in tandem devices *Sustain. Energy Fuels* **3** 2246–59
- [4] Gupta G K and Dixit A 2018 Theoretical studies of single and tandem $Cu_2ZnSn(S/Se)_4$ junction solar cells for enhanced efficiency *Opt. Mater.* **82** 11–20
- [5] Grossberg M, Krustok J, Raudoja J, Timmo K, Altosaar M and Raadik T 2011 Photoluminescence and Raman study of $Cu_2ZnSn(SexS_{1-x})_4$ monograins for photovoltaic applications *Thin Solid Films* **519** 7403–6
- [6] Grossberg M, Krustok J, Raudoja J and Raadik T 2012 The role of structural properties on deep defect states in Cu_2ZnSnS_4 studied by photoluminescence spectroscopy *Appl. Phys. Lett.* **101** 102102
- [7] Grossberg M, Krustok J, Raadik T, Kauk-Kuusik M and Raudoja J 2014 Photoluminescence study of disordering in the cation sublattice of Cu_2ZnSnS_4 *Curr. Appl. Phys.* **14** 1424–7
- [8] Kauk-Kuusik M *et al* 2018 Study of $Cu_2CdGeSe_4$ monograin powders synthesized by molten salt method for photovoltaic applications *Thin Solid Films* **666** 15–9
- [9] Grossberg M, Raadik T, Krustok J, Kauk-Kuusik M, Timmo K, Kaupmees R, Mikli V and Mere A 2018 Optical

- and structural properties of orthorhombic and tetragonal polymorphs of Cu₂CdGeSe₄ *Thin Solid Films* **666** 44–47
- [10] Litvinchuk A P, Dzhagan V M, Yukhymchuk V O, Valakh M Y, Babichuk I S, Parasyuk O V, Piskach L V, Gordan O D and Zahn D R T 2014 Electronic structure, optical properties, and lattice dynamics of orthorhombic Cu₂CdGeS₄ and Cu₂CdSiS₄ semiconductors *Phys. Rev. B* **90** 165201
- [11] Davidiyuk G E, Parasyuk O V, Semenyuk S A and Romanyuk Y E 2003 Electrical and optical properties of Cu₂CdGeS₄ single crystals *Inorg. Mater.* **39** 919–23
- [12] Zhang Y, Sun X, Zhang P, Yuan X, Huang F and Zhang W 2012 Structural properties and quasiparticle band structures of Cu-based quaternary semiconductors for photovoltaic applications *J. Phys. D: Appl. Phys.* **111** 063709
- [13] Brik M G, Kityk I V, Parasyuk O V and Myronchuk G L 2013 Photoinduced features of energy bandgap in quaternary Cu₂CdGeS₄ crystals *J. Phys. Condens. Matter.* **25** 505802
- [14] Parasyuk O V, Romanyuk Y E and Olekseyuk I D 2005 Single-crystal growth of Cu₂CdGeS₄ *J. Cryst. Growth* **275** e159–62
- [15] Huang S, Zai J, Ma D, He Q, Liu Y, Qiao Q and Qian X 2016 Colloidal synthesis of wurtz-stannite Cu₂CdGeS₄ nanocrystals with high catalytic activity toward iodine redox couples in dye-sensitized solar cells *Chem. Commun.* **52** 10866–9
- [16] Altosaar M, Danilson M, Kauk M, Krustok J, Mellikov E, Raudoja J, Timmo K and Varema T 2005 Further developments in CIS monograin layer solar cells technology *Sol. Energy Mater. Sol. Cells* **87** 25–32
- [17] Lavrentyev A A, Gabrelian B V, Vu V T, Shkumat P N, Ocheretova V A, Parasyuk O V and Khyzhun O Y 2015 Electronic structure and optical properties of Cu₂CdGeS₄: DFT calculations and X-ray spectroscopy measurements *Opt. Mater.* **47** 435–44
- [18] Himmrich M and Haeuseler H 1991 Far infrared studies on stannite and wurtzstannite type compounds *Spectrochim. Acta Part A: Mol. Spectrosc.* **47** 933–42
- [19] Kato H, Sato J, Abe T and Kashiwaba Y 2004 Photoluminescence of p-type CdS:Cu thin films *Phys. Status Solidi* **1** 653–6
- [20] Mandal P, Talwar S S, Major S S and Srinivasa R S 2008 Orange-red luminescence from Cu doped CdS nanophosphor prepared using mixed Langmuir-Blodgett multilayers *J. Chem. Phys.* **128** 114703
- [21] Schmidt T, Lischka K and Zulehner W 1992 Excitation-power dependence of the near-band-edge photoluminescence of semiconductors *Phys. Rev. B* **45** 8989–94
- [22] Krustok J, Raadik T, Grossberg M, Kauk-Kuusik M, Trifiletti V and Binetti S 2018 Photoluminescence study of deep donor- deep acceptor pairs in Cu₂ZnSnS₄ *Mater. Sci. Semicond. Process.* **80** 52–5R
- [23] Krustok J, Raudoja J, Krunks M, Mändar H and Collan H 2000 Nature of the native deep localized defect recombination centers in the chalcopyrite and orthorhombic AgInS₂ *J. Phys. D: Appl. Phys.* **33** 205–9
- [24] Krustok J, Raudoja J, Schön J H, Yakushev M and Collan H 2000 Role of deep donor-deep acceptor complexes in CIS-related compounds *Thin Solid Films* **361** 406–10
- [25] Krustok J, Schön J H, Collan H, Yakushev M, Mädasson J and Bucher E 1999 Origin of the deep center photoluminescence in CuGaSe₂ and CuInS₂ crystals *J. Phys. D: Appl. Phys.* **32** 364–9
- [26] Yakushev M V, Márquez-Prieto J, Forbes I, Edwards P R, Zhivulko V D, Mudryi A V, Krustok J and Martin R W 2015 Radiative recombination in Cu₂ZnSnSe₄ thin films with Cu deficiency and Zn excess *J. Phys. D: Appl. Phys.* **48** 475109
- [27] Krustok J, Collan H, Yakushev M and Hjelt K 1999 The role of spatial potential fluctuations in the shape of the PL bands of multinary semiconductor compounds *Phys. Scr.* **T79** 179
- [28] Krustok J, Raudoja J, Yakushev M, Pilkington R D D and Collan H 1999 On the shape of the close-to-band-edge photoluminescent emission spectrum in compensated CuGaSe₂ *Phys. Status Solidi* **173** 483–90
- [29] Krustok J, Collan H and Hjelt K 1997 Does the low-temperature Arrhenius plot of the photoluminescence intensity in CdTe point towards an erroneous activation energy? *J. Phys. D: Appl. Phys.* **30** 1442–5
- [30] Chen S, Walsh A, Gong X-G and Wei S-H 2013 Classification of lattice defects in the kesterite Cu₂ZnSnS₄ and Cu₂ZnSnSe₄ earth-abundant solar cell absorbers *Adv. Mater.* **25** 1522–39